

Origins of barchan dune asymmetry: insights from numerical simulations

Eric J. R. Parteli^a, Orencio Durán^b, Mary C. Bourke^{c,d}, Haim Tsoar^e, Thorsten Pöschel^a, Hans J. Herrmann^{f,g}

^a*Institut für Multiscale Simulation, Universität Erlangen-Nürnberg, Nägelsbachstr. 49b, 91052 Erlangen, Germany*

^b*MARUM — Center for Marine Environmental Sciences, University of Bremen, 28359 Bremen, Germany*

^c*Planetary Science Institute, 1700 E Ft Lowell, #106, Tucson AZ, USA*

^d*Department of Geography, Trinity College Dublin, Ireland*

^e*Dep. Geogr. Environ. Development, Ben-Gurion Univ. Negev, Beer Sheva 84105, Israel*

^f*Institut für Baustoffe IfB, ETH Hönggerberg, HIF E 12, CH-8093, Zürich, Switzerland.*

^g*Departamento de Física, Universidade Federal do Ceará - 60455-760, Fortaleza, Ceará, Brazil*

Abstract

Barchan dunes — crescent-shaped dunes that form in areas of unidirectional winds and low sand availability — commonly display an asymmetric shape, with one limb extended downwind. Several factors have been identified as potential causes for barchan dune asymmetry on Earth and Mars: asymmetric bimodal wind regime, topography, influx asymmetry and dune collision. However, the dynamics and potential range of barchan morphologies emerging under each specific scenario that leads to dune asymmetry are far from being understood. In the present work, we use dune modeling in order to investigate the formation and evolution of asymmetric barchans. We find that a bimodal wind regime causes limb extension when the divergence angle between primary and secondary winds is larger than 90° , whereas the extended limb evolves into a seif dune if the ratio between secondary and primary transport rates is larger than 25%. Calculations of dune formation on an inclined surface under constant wind direction also lead to barchan asymmetry, however no seif dune is obtained from surface tilting alone. Asymmetric barchans migrating along a tilted surface move laterally, with transverse migration velocity proportional to the slope of the terrain. Limb elongation induced by topography can occur when a barchan crosses a topographic rise. Furthermore, transient asymmetric barchan shapes with extended limb also emerge during collisions between dunes or due to an asymmetric influx. Our findings can be useful for making quantitative inference on local wind regimes or spatial heterogeneities in transport conditions of planetary dune fields hosting asymmetric barchans.

Keywords: Barchan dunes, Dune asymmetry, Wind erosion, Sand transport, Dune model

1. Introduction

The classical symmetric shape of barchan dunes is far from being prevalent in nature. A wide variety of barchan morphologies on Earth and Mars are asymmetric, with one extended limb (cf. Fig. 1) (Tsoar, 1984; Bourke, 2010). Since the pioneering works by Bagnold (1941), various conceptual models have been proposed in order to explain the existing asymmetric dune morphologies. Dune asymmetry has been most predominantly attributed to asymmetric bimodal winds (Bagnold, 1941; Tsoar, 1984), topography (Finkel, 1959; Long and Sharp, 1964), dune collisions (Close-Arceud, 1969; Hersen and Douady, 2005) or asymmetric sand influx (Rim, 1958). Indeed, understanding dune asymmetry constitutes an important issue in planetary science, as asymmetric dunes could potentially serve as a proxy for local wind regimes or variations in sand supply or topography. However, the significance of the different causes of barchan asymmetry is still poorly understood, whereas the potential range of dune morphologies

resulting in each case remains unknown. Although some insights into the dynamics of asymmetric dunes could be gained from field monitoring within a time span of a few years (Bourke, 2010), assessment of dune shape evolution is a difficult task owing to the long timescales involved in dune processes. Moreover, diverse asymmetric dune morphologies (Bourke et al., 2004; Bourke and Goudie, 2009) might be the outcome of different factors in concurrent action, which poses a further challenge in the investigation of the developmental stages of asymmetric dunes through field observations.

Numerical modeling — which has become indispensable in the investigation of aeolian and dune processes on Earth and other planetary bodies (Bourke et al., 2010; Kok et al., 2012) — could provide a helpful tool in the study of barchan dune asymmetry. In order to shed light on the factors competing for the appearance of various asymmetric dune shapes, a minimal model that accounts for a mathematical description of the wind over dunes, as well as for the equations for grain transport and landscape evolution is required. Such a model has been developed in the course of the last decade (Sauermaun et al.,

Email address: Eric.Parteli@cbi.uni-erlangen.de (Eric J. R. Parteli)

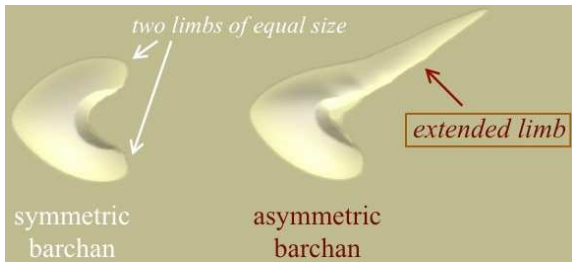


Figure 1: Schematic diagram of a symmetric barchan with two limbs of equal size (left) and of an asymmetric barchan with an extended limb (right).

2001; Kroy et al., 2002; Durán and Herrmann, 2006a; Durán et al., 2010). This model combines an analytical model for the average turbulent flow over the sand landscape with a continuum model for sand transport. The model has proven to reproduce the shape of different types of dunes with good quantitative agreement with measurements (Sauermann et al., 2003; Durán and Herrmann, 2006a,b; Parteli and Herrmann, 2007). The model has been further extended in order to model longitudinal seif dunes and diverse unusual Martian dune forms under bimodal wind regimes (Parteli et al., 2009).

In the present work, we use the dune model to investigate the role of different asymmetry causes for the diversity of asymmetric barchan shapes reported previously from observations of dune fields on Earth and Mars (Bourke, 2010). We calculate the evolution of a symmetric barchan dune under the separate action of the potential causes for dune asymmetry.

This paper is organized as follows. In Section 2 the dune model is described. In Sections 3-6 we present the results obtained from calculations of barchan dune asymmetry due to bimodal wind regimes, topography, asymmetric sand supply and dune collision, respectively. Moreover, in Section 7 we compare the results of our simulations with the shapes of real asymmetric barchans and discuss on the application of the model outcomes to the research of extraterrestrial dunes. Finally, conclusions are presented in Section 8.

2. Model description

The model used in the calculations of the present work consists of a set of mathematical equations that compute: the average turbulent wind field (the surface shear stress ($\boldsymbol{\tau}$) over the topography; the mass flux (\boldsymbol{q}) of saltating particles due to the shear stress, and the time evolution of the surface resulting from particle transport (Sauermann et al., 2001; Kroy et al., 2002; Durán and Herrmann, 2006a). In this Section, we present a brief description of the model equations and of the calculation procedure.

2.1. Wind field

The first step of the model calculations consists of describing quantitatively the average three-dimensional turbulent wind field over the dune. The average shear stress field ($\boldsymbol{\tau}$) is calculated through solving a set of analytical equations developed by Weng et al. (1991).

In the absence of dunes, the wind velocity $\boldsymbol{v}(z)$ within the atmospheric boundary layer increases logarithmically with the height (z) above the flat ground. That is,

$$\boldsymbol{v}(z) = [\boldsymbol{u}_{*0}/\kappa] \ln(z/z_0), \quad (1)$$

where $\kappa = 0.4$ is the von Kármán constant and \boldsymbol{u}_{*0} is the wind shear velocity, which is used to define the (undisturbed) shear stress $\boldsymbol{\tau}_0 = \rho_{\text{fluid}} |\boldsymbol{u}_{*0}| \boldsymbol{u}_{*0}$, with ρ_{fluid} standing for the air density (Bagnold, 1941; Sullivan et al., 2000). Furthermore, z_0 is the surface roughness, which scales with the average grain size (d) composing the sand bed. We take $z_0 \approx d/20$ based on a recent theoretical work on modeling saturated sand flux (Durán and Herrmann, 2006a).

A smooth hill or dune introduces a perturbation in the wind field. The Fourier-transformed longitudinal and transverse components of the shear stress perturbation ($\hat{\boldsymbol{\tau}}$) due to the local topography are computed using following equations,

$$\tilde{\hat{\tau}}_x = \frac{\tilde{h}_s k_x^2}{|\vec{k}|} \frac{2}{U^2(l)} \left\{ -1 + \left(2 \ln \frac{l}{z'_0} + \frac{|\vec{k}|^2}{k_x^2} \right) \sigma \frac{K_1(2\sigma)}{K_0(2\sigma)} \right\}, \quad (2)$$

$$\tilde{\hat{\tau}}_y = \frac{\tilde{h}_s k_x k_y}{|\vec{k}|} \frac{2}{U^2(l)} 2\sqrt{2}\sigma K_1(2\sqrt{2}\sigma), \quad (3)$$

where x and y are parallel, respectively, perpendicular to the wind direction, $\sigma = \sqrt{iLk_x z_0/l}$, k_x and k_y are the components of the wave vector \vec{k} , i.e. the coordinates in Fourier space, K_0 and K_1 are modified Bessel functions and \tilde{h}_s is the Fourier transform of the height profile; U is the vertical velocity profile which is suitably non-dimensionalized, l is the depth of the inner layer of the flow and L is a typical length scale of the hill or dune and is given by 1/4 the mean wavelength of the Fourier representation of the height profile. In the presence of the saltating grains, the roughness of the dune's surface increases to an apparent value z'_0 , the aerodynamic roughness (Bagnold, 1941). The wind velocity over the dune is calculated using $z'_0 = 1$ mm, a value based on experimental observations (Bagnold, 1941; Andreotti, 2004). The surface shear stress field is obtained, then, with the equation,

$$\boldsymbol{\tau} = |\boldsymbol{\tau}_0| (|\boldsymbol{\tau}_0|/\boldsymbol{\tau}_0 + \hat{\boldsymbol{\tau}}), \quad (4)$$

where $\boldsymbol{\tau}_0$ is the undisturbed shear stress over the flat ground.

Flow separation at the dune brink due to the strong local curvature of the surface gives rise to a zone of recirculating flow (Walker and Nickling, 2002; Herrmann et al.,

2005; Araújo et al., 2013), which cannot be described by the analytical model (Weng et al., 1991). This problem is overcome introducing the so-called “separation bubble”: for each longitudinal slice of the dune, a separation streamline connecting the brink to the reattachment point is introduced at the lee. Each separation streamline is fitted to a third-order polynomial, the parameters of which are determined as described in detail by Kroy et al. (2002). The wind model (Weng et al., 1991) is then solved for the smooth “envelope” that comprises the separation bubble and the dune surface (Kroy et al., 2002). Thereafter, the shear stress in the recirculating zone within the separation bubble is set as zero, since the net transport within the bubble essentially vanishes.

2.2. Sand flux

Next, the mass flux of particles in saltation — which is the dominant transport mode and consists of grains hopping in ballistic trajectories and ejecting new particles upon collision with the ground — is computed. The saltation cloud is regarded as a thin, fluid-like layer that can exchange sand with the immobile sand bed (Sauermaun et al., 2001).

When the wind shear stress exceeds a minimal threshold and saltation begins, the sand flux first grows exponentially due to the multiplicative process inherent to the saltation process. However, since saltating grains accelerate at cost of aeolian momentum, the flux cannot increase beyond a maximal value, the so-called saturated sand flux (Bagnold, 1941; Sauermaun et al., 2001; Almeida et al., 2008; Durán et al., 2011; Pähtz et al., 2012) which is reached after a saturation transient where the air shear stress within the saltation cloud equals the minimal value for sustained saltation, i.e. the impact threshold, $\tau_t = \rho_{\text{fluid}} u_{*t}^2$ (Bagnold, 1941), defined in terms of the impact threshold shear velocity u_{*t} . In the continuum model, the derivation of the three-dimensional equations for the sand flux is performed by explicitly accounting for the decrease in aeolian shear stress due to the growth of the number of particles in saltation (the “feedback effect” (Owen, 1964)), which leads to the saturation transient of the flux as described above. The following equation is obtained for the sand flux (\mathbf{q}) over the terrain,

$$\nabla \cdot \mathbf{q} = (1 - |\mathbf{q}|/q_s) |\mathbf{q}|/\ell_s, \quad (5)$$

where $q_s = [2\alpha |\mathbf{v}_s|/g](\tau - \tau_t)$ is the saturated flux; $\ell_s = [2\alpha |\mathbf{v}_s|^2/g\gamma]\tau_t(\tau - \tau_t)^{-1}$ is the characteristic length of flux saturation; g is gravity; $\alpha \approx 0.4$ and $\gamma \approx 0.2$ are empirically determined model parameters (Sauermaun et al., 2001; Durán and Herrmann, 2006a), and the steady-state velocity of the particles in saltation (\mathbf{v}_s) is calculated numerically from the balance between aeolian drag, gravitational and bed friction forces on the particles (Durán et al., 2010). The outcome of the calculation is a two-dimensional field ($\mathbf{q}(x, y)$) that gives the height-integrated, average mass flux of saltating particles over the terrain.

2.3. Surface evolution

Finally, mass conservation is used in order to compute the evolution of the local height ($h(x, y)$) through the equation,

$$\rho_{\text{sand}} \partial h / \partial t = -\nabla \cdot \mathbf{q}, \quad (6)$$

where ρ_{sand} is the bulk sand density. Eq. (6) implies that the deposition (erosion) occurs at those places where the flux locally decreases (increases) downwind.

Avalanches — wherever the local slope exceeds the angle of repose of the sand ($\theta_c \approx 34^\circ$), the surface is relaxed through avalanches in the direction of the steepest descent. Avalanches are considered to be instantaneous as their time-scale can be regarded as negligible compared to the time-scale of the surface evolution due to aeolian transport. The flux of avalanches along the slip-face is given by,

$$\mathbf{q}_{\text{aval}} = k [\tanh(\nabla h) - \tanh(\theta_{\text{dyn}})] \frac{\nabla h}{|\nabla h|}, \quad (7)$$

where $k = 0.9$ is a parameter and $\theta_{\text{dyn}} = 33^\circ$ is the so-called “dynamic” angle of repose, which characterizes the surface after relaxation (Durán et al., 2010). The update in the local height is obtained by solving Eq. (6) using the flux due to avalanches given by Eq. (7). The calculation is repeated until the local slope is below θ_{dyn} .

2.4. Description of the calculation procedure

Summarizing, the model consists of iteratively performing the following calculations:

1. the average shear stress (τ) over the surface is computed using Eqs. (2), (3) and (4);
2. next, the height-integrated average mass flux \mathbf{q} over the terrain is calculated by solving Eq. (5);
3. the change in the local surface is computed with Eq. (6); wherever the local inclination is larger than 34° , the flux due to avalanches is calculated using Eq. (7) and the topography updated again using Eq. (6).

The initial surface is a smooth hill of Gaussian shape, which is subjected to a constant upwind shear stress of value τ_0 — in the following, we call the upwind shear stress simply τ .

Calculations are performed with open boundaries and an influx q_{in} at the inlet, which is a fraction of the saturated flux, q_s . Indeed, field observations show that transport in interdune areas is typically in the undersaturated regime and is dependent upon several factors, predominantly terrain type and the size and shape of dunes upwind (Fryberger et al., 1984). We consider that the interdune flux in a field of barchans migrating on top of bedrock is dictated by the average output flux of the dunes in the field (that is, the flux of sediment being released from the barchans’ limb). Since the output flux of barchan dunes produced with the model is about 20% of the saturated flux (Durán et al., 2010), we choose $q_{\text{in}}/q_s = 0.2$. We

note that this choice for q_{in}/q_s is fairly consistent with measurements of drift rates by Fryberger et al. (1984) in the Jafurah sand sea in Saudi Arabia. The authors reported monthly-averaged drift rates downwind of a mature barchan varying within a broad range between 0 and about 67% of the value on top of a sand sheet (where the flux is saturated), with annual mean about 20% (cf. data for trap #6 in Table 2 by Fryberger et al. (1984)). However, we further note that the same authors also reported significantly larger drift rates (about 60%) downwind of domes and small dunes with incipient slip-face, while nearly vanishing drift rate values were obtained from measurements in interdune areas consisting of salt-encrusted sandy plains. Therefore, it should be remarked that our choice for q_{in} should be reasonable for mature barchans separated by bedrock interdune areas. For other situations, like dunes surrounded by sand patches that can serve as sediment source or evolving on a terrain containing vegetation or moisture (thus hindering interdune sediment transport), the value of q_{in} should be adjusted in order to adequately model the particular physical conditions.

A list of the main relevant parameters of the model with their respective values used in our calculations is displayed in Table 1.

3. Bimodal wind regimes

Most attempts to model barchan asymmetry have concentrated on the role of asymmetric bimodal wind regimes for the elongation of one barchan limb (Bagnold, 1941; Tsoar, 1984) (see also Bourke (2010)). The bimodal wind is said to be asymmetric when the transport rates of both wind components are not equal.

The first conceptual model was by Bagnold (1941). According to this model, a symmetric barchan, originally formed by a gentle wind, becomes asymmetric if a storm wind blows from a secondary direction, making an acute divergence angle with the primary one. The limb exposed to the storm wind elongates as it enters the sand stream of the limb at the opposite side, thus evolving into a longitudinal seif dune (McKee and Tibbitts, 1964; Tsoar, 1982, 1983; Bristow et al., 2000; Rubin et al., 2008; Tokano, 2010). According to Bagnold’s model, the seif dune formed in this manner aligns approximately parallel to the direction of the storm (Bagnold, 1941). This conceptual model was referred to by many authors in the past (Verstappen, 1968; Ruhe, 1975; Goudie and Wilkinson, 1977; Mabbutt, 1977; Lancaster, 1980), though reports on supporting field examples were scarce (Lancaster, 1980). A different model was proposed later by Tsoar (1984): a gentle wind (not a storm wind) blows from the secondary direction, and the limb that elongates is the one opposite to the secondary gentle wind (Tsoar, 1984). Some field observations exist that support this model (Bourke, 2010).

In our calculations, we simulate a bimodal wind by periodically alternating the orientation of the field between two directions forming a divergence angle, θ_w

(Parteli et al., 2009) — such as in the turntable experiments of ripples and subaqueous dune formation on a sediment bed under bimodal flow regimes (Rubin and Hunter, 1987; Rubin and Ikeda, 1990). The wind model is solved considering a constant wind blowing over the rotated landscape, while the separation bubble adapts to the wind direction following the rotation of the field (Parteli et al., 2009). The *primary* wind direction, i.e. the one that forms the barchan, has duration T_{w1} and upwind shear stress τ_1 . The *secondary* wind direction makes an angle θ_w with the primary wind, and lasts for a time T_{w2} with upwind shear stress τ_2 .

We begin our study with an obtuse divergence angle ($\theta_w = 120^\circ$), and consider two models:

Model #1: both wind directions have the same upwind shear stress ($\tau_1 = \tau_2$), however the primary wind has a longer duration ($T_{w1} > T_{w2}$) — a scenario reminiscent of the experiments by Rubin and Hunter (1987) with the difference, however, that in the simulations the ground is not covered with sand. Fig. 2 shows snapshots of the dune evolution obtained from the calculations. As can be seen from Fig. 2, the barchan develops an asymmetric shape, which depends on the ratio $r \equiv T_{w2}/T_{w1}$. If $r > 25\%$, then the limb at the side opposite to the secondary wind elongates into the *resultant* wind direction (Fig. 2) to form a longitudinal dune. It is interesting that the longitudinal alignment also appears to be lost in turntable experiments of ripples on a sand bed when the transport rates differ by a factor larger than 4 (Rubin and Hunter, 1987). A theoretical model following the concept of maximum gross transport (Rubin and Hunter, 1987; Rubin and Ikeda, 1990) could shed light on the origin of the threshold value of r for seif dune elongation. Here we could not find a significant dependence of this threshold on θ_w or q_{in} . When $r = 1.0$, the barchan dune gives place to a symmetric longitudinal dune (Parteli et al., 2009).

Model #2: the primary wind has a larger shear stress ($\tau_1 > \tau_2$) — as in the conceptual model by Tsoar (1984) — while $T_{w1} = T_{w2}$. In this case, the dune shapes do not differ much from the ones in Fig. 2. The limb opposite to the secondary wind elongates when the relative values of bulk sand flux in the secondary and primary wind directions, respectively Q_2 and Q_1 , are such that $r \equiv Q_2/Q_1 > 25\%$. Indeed, we also considered the situation where the storm wind is the secondary one ($Q_2 > Q_1$), such as in the model by Bagnold (1941). In this case, primary and secondary winds simply exchange their roles, whereas the same dune shapes such as in Fig. 2 are obtained. In summary, Bagnold’s hypothesis that the elongating limb is the one exposed to a secondary storm wind is not supported by the simulation results.

In a general manner, the condition for elongation of the asymmetric limb due to a bimodal wind of obtuse divergence angle, as found from our calculations, reads:

$$r \equiv [Q_2 \cdot T_{w2}]/[Q_1 \cdot T_{w1}] > 1/4, \quad (8)$$

where the indices 1 and 2 refer to the primary and to the

d (μm)	ρ_p (kg/m^3)	η ($\text{kg}/\text{m}\cdot\text{s}$)	ρ_{fluid} (kg/m^3)	g (m/s^2)	z_0 (μm)	z'_0 (m)	α	γ
250	2650	1.78×10^{-5}	1.225	9.8	1.25	0.001	0.4	0.2

Table 1: Main relevant parameters of the model with their respective values associated with aeolian transport under Earth conditions (Sauermann et al., 2001; Kroy et al., 2002; Durán and Herrmann, 2006a; Durán et al., 2010). $d = 250\mu\text{m}$ is the average grain size of Earth dunes (Pye and Tsoar, 1990) and $\rho_p = 2650\text{kg}/\text{m}^3$ is the density of quartz, while $\rho_{\text{fluid}} = 1.225\text{kg}/\text{m}^3$ and $\eta = 1.78 \times 10^{-5}\text{kg}\text{m}^{-1}\text{s}^{-1}$ are the density and dynamic viscosity of the air, respectively. Furthermore, $g = 9.81\text{m}/\text{s}^2$ is gravity, $z_0 \approx d/20 = 1.25\mu\text{m}$ is the surface roughness in the absence of saltation and $z'_0 = 1\text{mm}$ is the aerodynamic roughness, which accounts for the presence of saltating cloud, while $\alpha = 0.4$ and $\gamma = 0.2$ are empirically determined parameters of the sand flux model (Sauermann et al., 2001; Durán and Herrmann, 2006a). Using these parameters, the threshold shear velocity for sustained transport, $u_{*t} \approx 0.21\text{m}/\text{s}$ is calculated with the model by Iversen and White (1982).

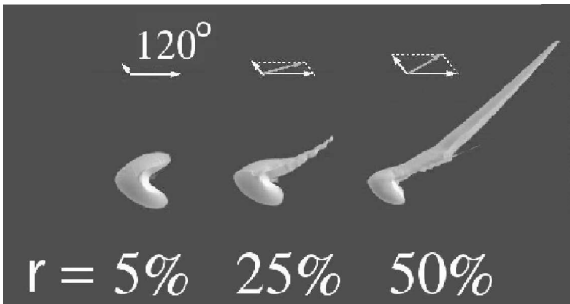


Figure 2: Elongation of one barchan limb due to a bimodal wind regime with obtuse divergence angle. Wind directions are indicated by the arrows (the primary wind, which has duration T_{w1} , blows from the left). The barchan shape depends on $r = T_{w2}/T_{w1}$, i.e. the duration T_{w2} of the secondary wind relative to T_{w1} . In these simulations, T_{w1} is about 3% of the migration time of the barchan dune, T_m . The shapes shown for $r \leq 25\%$ are *stationary* shapes, whereas for $r > 25\%$, the elongated dune horn increases with time. Simulation snapshots correspond to time t of the order of $5T_m$. The barchan obtained in the simulation with $r = 5\%$ has length and width of approximately 120 m.

secondary wind, respectively. Equation (8) allows us to estimate the onset for emergence of asymmetry in barchan dunes, where both the relative duration and shear stress values of the wind components are accounted for quantitatively.

Next, we extend the calculations to different values of the divergence angle θ_w . In Fig. 3, the dune shape emerging from an asymmetric bimodal wind with $r = 50\%$ is shown as a function of θ_w and $t_1 = T_{w1}/T_m$, which is the duration of the primary wind, T_{w1} , rescaled by the migration or reconstitution time of the barchan, $T_m \approx 0.02W^2/Q_1$ (Durán et al., 2010). The dune turnover time is roughly the time needed for the dune to cover a distance of its width (W) (Allen, 1974; Lancaster, 1988; Rubin and Ikeda, 1990; Hersen et al., 2004).

As can be seen from Fig. 3, dunes orient transversely or

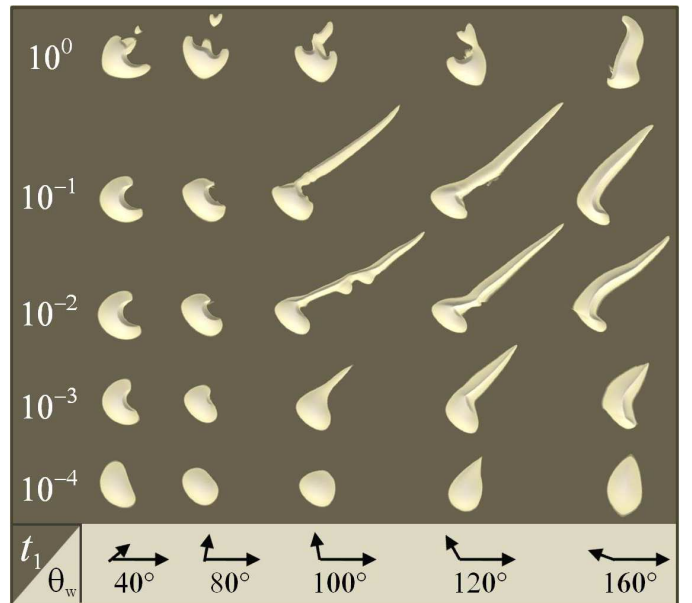


Figure 3: Dune shape as a function of the divergence angle (θ_w) of the bimodal wind, and of the rescaled duration of the primary wind ($t_1 \equiv T_{w1}/T_m$), for $r = 50\%$, where $r \equiv T_{w2}/T_{w1}$ is the ratio between the duration T_{w2} of the secondary wind and the duration of the primary wind (T_{w1}). The directions of primary and secondary winds are indicated by the arrows (primary wind blows to the right). Simulation snapshots correspond to time $t \approx 3T_m$, except those obtained with $t_1 = 10^{-4}$, which correspond to time $t \approx 0.2T_m$.

longitudinally to the resultant transport trend, depending on whether θ_w is acute or obtuse, respectively. Bimodal wind regimes with $\theta_w < 90^\circ$ lead to rounded (or oblate) barchans, whereas larger values of θ_w yield asymmetric dunes that elongate in the resultant transport direction (Parteli et al., 2009). However, the elongating limb is not stable if θ_w is within the range $90^\circ < \theta_w \lesssim 112^\circ$. In this case, if the influx is sufficiently small, the extended limb separates from the barchan, giving rise to a “mixed

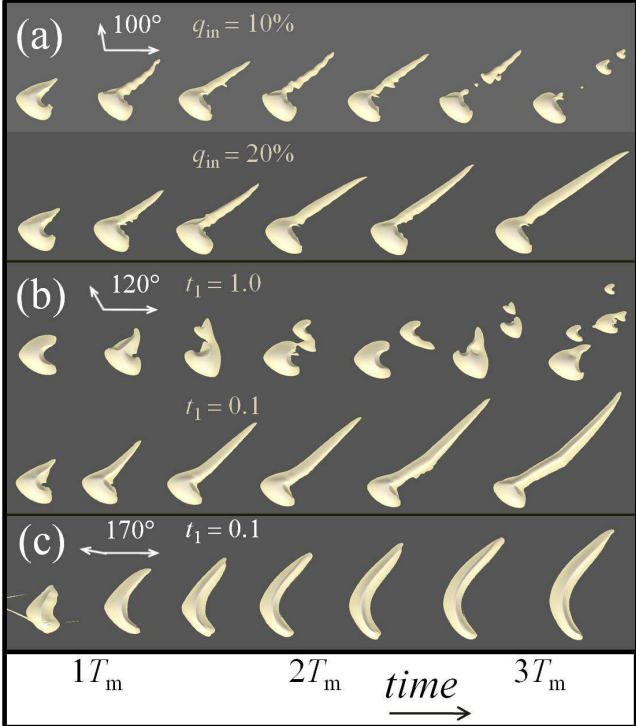


Figure 4: Time evolution of the barchan shape under bimodal wind regimes with obtuse divergence angle and $r = 50\%$ (cf. Fig. 3). Time is in units of the turnover time of the barchan (T_m). (a) The divergence angle is $\theta_w = 100^\circ$, the duration of the primary wind (to the right) relative to T_m is $t_1 = 0.1$, and the influx (q_{in}) is 10% (top) and 20% (bottom); (b) $\theta_w = 120^\circ$, $q_{in} = 20\%$, $t_1 = 1.0$ (top) and 0.1 (bottom); (c) $\theta_w = 170^\circ$, $q_{in} = 20\%$, $t_1 = 0.1$.

state” (Rubin and Hunter, 1987; Rubin and Ikeda, 1990; Parteli et al., 2009), as depicted in Fig. 4a. In fact, mixed states analogous to the ones found for asymmetric barchans have been also found in turntable experiments of aeolian ripples and subaqueous bedforms on a sand bed for the same range of θ_w (Rubin and Hunter, 1987; Rubin and Ikeda, 1990). At very large divergence angles, the resulting morphology resembles an asymmetric dune of “slim” shape (Long and Sharp, 1964; Bourke, 2010), as shown in the diagram of Fig. 3 and also illustrated with the calculation using $\theta_w = 170^\circ$ in Fig. 4c. The dunes in Fig. 4c are “reversing” dunes, which are formed by winds coming from opposing directions. This dune form has been discussed by Tsoar (2001), who also gave examples of reversing dunes occurring in South Africa (Tsoar, 2001).

Asymmetric barchans such as the ones in Fig. 2 form when the relative duration of the primary wind ($t_1 \equiv T_{w1}/T_m$) is within the range $10^{-3} \lesssim t_1 \lesssim 10^{-1}$. When t_1 is smaller than about 0.1%, no limb elongation occurs; both limbs, as well as the slip face, disappear and a dome-like shape is obtained (cf. Fig. 3). As t_1 approaches unity, any change due to the secondary wind is fully compensated

by the primary wind during every cycle of the bimodal wind regime — the resulting morphology is essentially a barchan that is periodically reformed by a unimodal wind of strength τ_1 , as can be seen from Fig. 3. The dune shapes shown in Fig. 3 for $t_1 = 1.0$ are thus “transitional” shapes (de Hon, 2006). The oblique incidence of the secondary wind leads to destabilization of the dune surface and the emergence of smaller barchans, which detach from the larger dune and migrate on the bedrock thereby alternating between both directions of the bimodal wind. Figure 4b shows the calculation of a barchan under asymmetric bimodal wind regime with $\theta_w = 120^\circ$ for $t_1 = 1.0$ (top) and $t_1 = 0.1$ (bottom). On the basis of Fig. 4b, it is possible to understand the coexistence of barchans and other complex bedforms shaped by multimodal wind regimes. If the dune is small enough, it has a small turnover time (\sim large t_1) and can readapt to the prevailing transport trend notwithstanding the complexity of the wind system (Lancaster, 1988).

4. Topography

Field evidence of barchan limb elongation caused by topography are unclear (Finkel, 1959; Long and Sharp, 1964; Gay, 1999; Bourke, 2010). We investigate two cases where topography is observed to trigger dune asymmetry under both constant wind direction and sediment supply.

Sloping terrain — We consider a barchan dune migrating on a sloping terrain that makes an angle φ with the horizontal (Fig. 5a). The simulation starts with a symmetric barchan of height H and width W , which was shaped on a flat surface under constant upwind shear stress τ and constant influx ($q_{in}/q_s = 0.2$). Then, the barchan is let to evolve on the inclined surface. Due to gravity, sand transport on the tilted surface has now a component perpendicular to wind trend.

Figure 5b shows that the emerging barchan shape is asymmetric, yet none of its limbs elongate to form a longitudinal dune (Parteli et al., 2009; Reffet et al., 2010). The asymmetry arises from the combined effect of both downwind sand transport and gravity-driven mass flow in the direction orthogonal to the wind. Sand transport along the lower limb has a small net component downhill due to the tilting, and so this limb stretches downhill. In contrast, the upper limb is not stretched because the sand transported laterally due to the tilting is trapped at the slip face.

A consequence of the surface inclination is the downhill extension of the barchan. The migration velocity of the barchan dune orthogonal to the wind trend increases with φ , as shown in the main plot of Fig. 5c. For moderate values of φ within the range $0 \leq \tan\varphi \leq 0.4$, the ratio between transverse and longitudinal migration velocities, v_T and v_L , respectively, can be described by the equation:

$$v_T/v_L = k_q \tan\varphi, \quad (9)$$

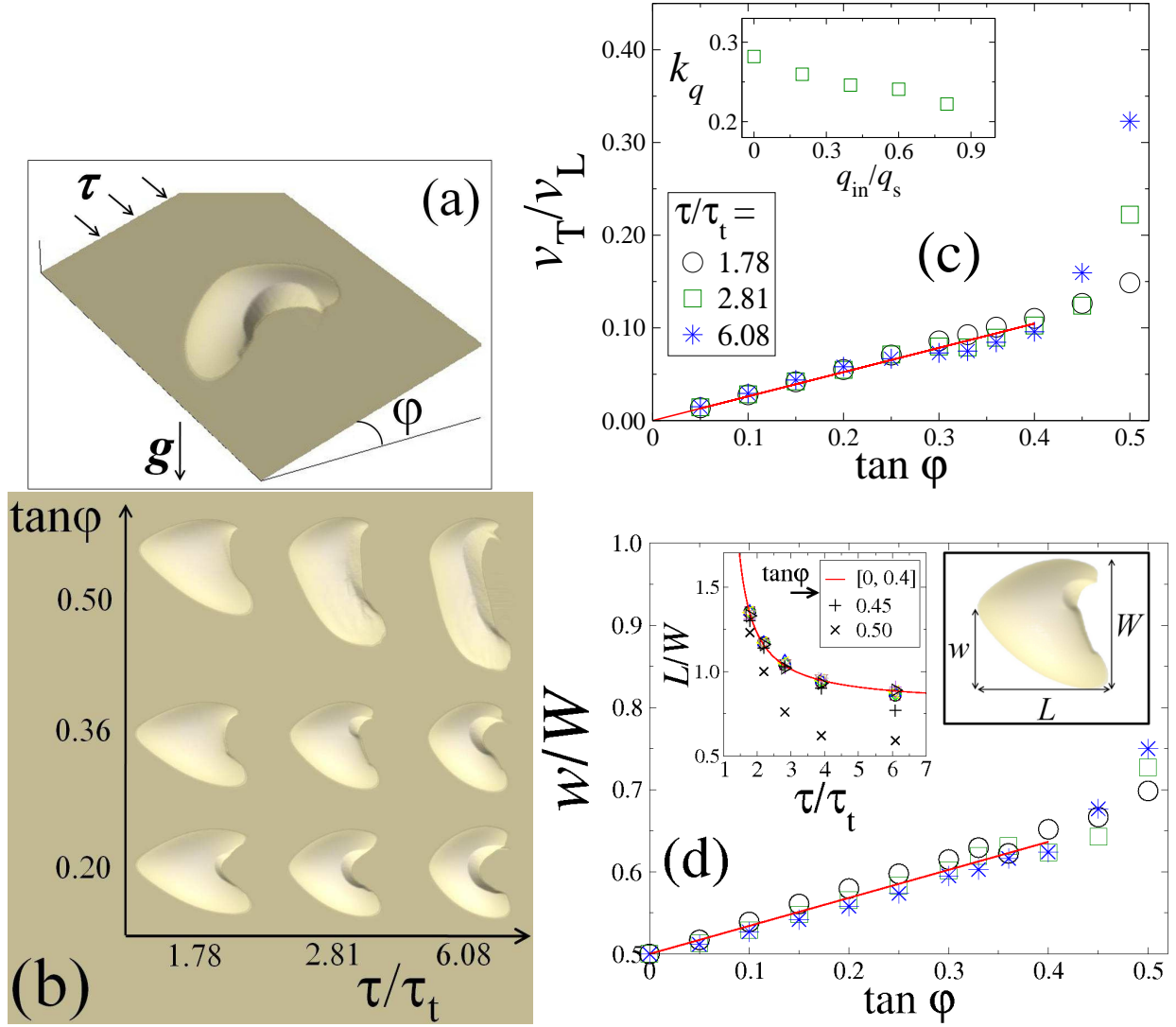


Figure 5: **(a)** Barchan dune of cross-wind width $W \approx 90$ m migrating along a sloping terrain. The surface is tilted by an angle φ . Arrows indicate the wind direction (τ is the upwind shear stress) and gravity (g). **(b)** Dune shape as a function of φ and τ/τ_t (wind blows from left to right). Simulations were performed with $q_{in}/q_s = 0.2$. **(c)** Main plot: Ratio between transverse and longitudinal migration velocities, respectively v_T and v_L . The best fit to the data using the equation $v_T/v_L = k_q \tan \varphi$ gives $k_q \approx 0.26$ (continuous line). Inset: k_q as a function of q_{in}/q_s . **(d)** Main plot: The degree of asymmetry is quantified in terms of the ratio w/W , calculated as a function of the surface inclination (φ) and for the same values of τ/τ_t shown in the main plot of (a). Inset: Length-to-width ratio (L/W) as a function of τ/τ_t calculated for different values of φ within the range $0 < \tan \varphi < 0.4$ and for two values of φ above this range ($\varphi = 0.45$ and $\varphi = 0.50$). The best fit to the data within the range $0 < \tan \varphi < 0.4$ using the equation $L/W \approx A[\tau/\tau_t - 1]^{-1} + B$ gives $A \approx 0.42$ and $B = 0.8$ (continuous line).

where the coefficient $k_q \approx 0.26$ has a slight dependence on the upwind sand flux, q_{in}/q_s (cf. inset of Fig. 5c). The ratio v_T/v_L for barchans migrating on a sloping terrain is thus a function of the slope φ , being independent of the wind velocity.

The topography-induced barchan asymmetry can be quantified in terms of the relative width w/W , where W is the total dune width, and the width w is the distance

— measured in the direction orthogonal to wind trend — between the border of the dune at the lowest elevation and the dune’s windward foot (cf. Fig. 5d). If there is no surface tilting ($\varphi = 0$), then $w/W = 0.5$ since the dune is symmetric along its central axis. As φ increases within the range $0 \leq \tan \varphi \leq 0.4$, w increases roughly linearly with $\tan \varphi$, as shown in Fig. 5d. Within this moderate range of

φ , the ratio w/W can be described by the equation,

$$w/W = k_w \tan \varphi, \quad (10)$$

where the value $k_w \approx 0.33$ is obtained from the best fit to the simulation data (cf. Fig. 5d). The aspect ratio of the dune (L/W), which is a function of the relative shear stress (τ/τ_t) (Kroy et al., 2002; Parteli et al., 2007), is essentially independent of φ . In other words, τ/τ_t and φ can be approximately estimated from L/W and w/W of the asymmetric barchan shape, respectively, provided other asymmetry causes (i.e. bimodal wind, dune collisions or influx asymmetry) are not relevant at the dune field considered.

Topographic rise — Asymmetric barchans occasionally occur approaching and crossing a topographic break in slope (Bourke, 2010). We investigate, using the dune model, the evolution of a barchan crossing a ridge that is placed obliquely to the direction of motion (Fig. 6). The dune is subjected to a unimodal wind regime and an influx that is 20% of the saturated flux. We consider that the longitudinal axis of the ridge forms a moderate angle with the direction orthogonal to the wind (about 45°). The ridge has Gaussian cross section, width L_r and height H_r , while the barchan has a height $H \approx 9$ m.

Indeed, the height-to-width ratio H_r/L_r (or aspect ratio) of the ridge cannot be too large, as the ridge would act as a barrier for sand transport. On the contrary, a ridge of too small aspect ratio has negligible effect on the dune shape. An asymmetric dune shape with limb elongation occurs when the aspect ratio of the ridge is about $1/20$. In Figs. 6b and 6c, the ridge has height $H_r = 7$ m and width $L_r \approx 150$ m. We have examined satellite images of the dune field of Fig. 6a and noted that the cross section of the low ridges can indeed vary within the broad range between 50 and 150 m. Thus, both in the field and in the simulations, the ridge’s cross section is of the same order of the cross-wind width of the barchan dune. As the barchan approaches the ridge, deposition occurs at the lee of the ridge, on the side corresponding to the closest limb. This limb then elongates once it arrives at the lee of the obstacle. The taller the ridge, the more accentuated the extension. As the other limb approaches sufficiently close to the ridge, a similar process occurs and thus that limb also elongates.

The deposition at the ridge’s lee occurs due to a decrease in wind strength just downwind of the crest. When the sand released through the limbs crosses the ridge’s crest, it cannot escape the lee since the transport rate there is reduced. As the dune advances and more limb sand is deposited, the wind strength at the lee suffices to extend the limb, yet accumulation ensues. Thus, from the sand released through this limb, a sand patch forms downwind of the ridge’s crest (second frame from left to right), which develops into an elongated limb (cf. third and fourth frames). Then, in the fifth frame, the left limb is crossing the ridge’s crest which also leads to a sand patch in the

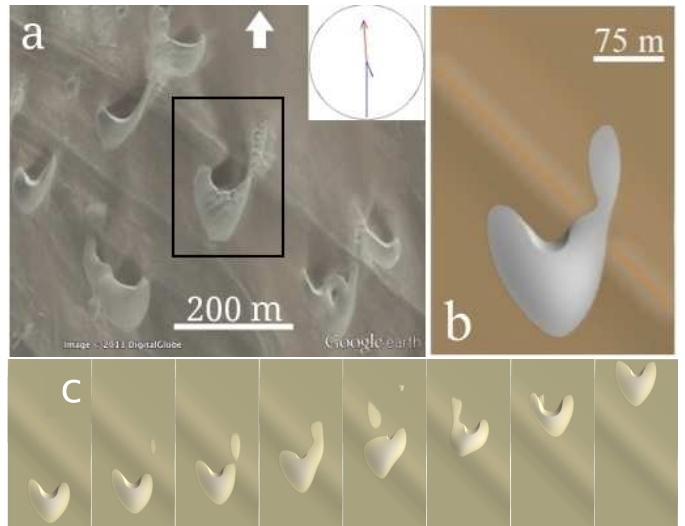


Figure 6: The potential influence of topography in the development of barchan asymmetry in Peru. (a) Barchan dunes migrating across a landscape where resistant layers in underlying bedrock protrude as low ridges. The dunes in the image are located near $14^\circ 52' 26.43''\text{S}$, $75^\circ 30' 58.31''\text{W}$. Illumination is from the top and the arrow indicates the north direction. The box indicates a barchan that extends its eastern limb across the topographic rise. The sand rose at the top-right corner is for San Juan de Marcona, located near $15^\circ 21'\text{S}$, $75^\circ 09'\text{W}$, about 68 km from the dunes in the image. Wind regime in the area is bimodal resulting in the extension of western limbs, except where influenced by topography. Image credit: Google Earth. (b) Asymmetric barchan dune of height ~ 9 m produced with the model using a topographic rise of Gaussian cross section which has along-wind width 200 m and height 6 m. (c) Simulation snapshots of the evolution of the barchan dune. Time increases from left to right and wind blows from the bottom. The simulation was performed with $\tau/\tau_t \approx 3.9$ and $q_{in}/q_s = 0.2$.

ridge’s wake. This process causes, then, elongation of the left limb as we can see in the subsequent frame.

It is interesting to note that in Fig. 6a not all barchans elongate the same limb. For instance, some barchans which have the right (left) limb elongated are upwind (downwind) of the ridge’s crest, which is in agreement with the prediction of Fig. 6c as discussed above. However, this behavior can be explained only if we assume that the dunes are well isolated from each other (i.e. they are not participating at a collision). For instance, the dune shape in the most lower right of Fig. 6a, which seems to result from a collision between dunes, has limbs of nearly equal size. Furthermore, the dune on the most lower left has an elongated arm opposite to that of the example barchan with the black box drawn around it. However, the elongated arm of the lower left dune too has a slip face — possibly indicating that this dune too is being affected by a

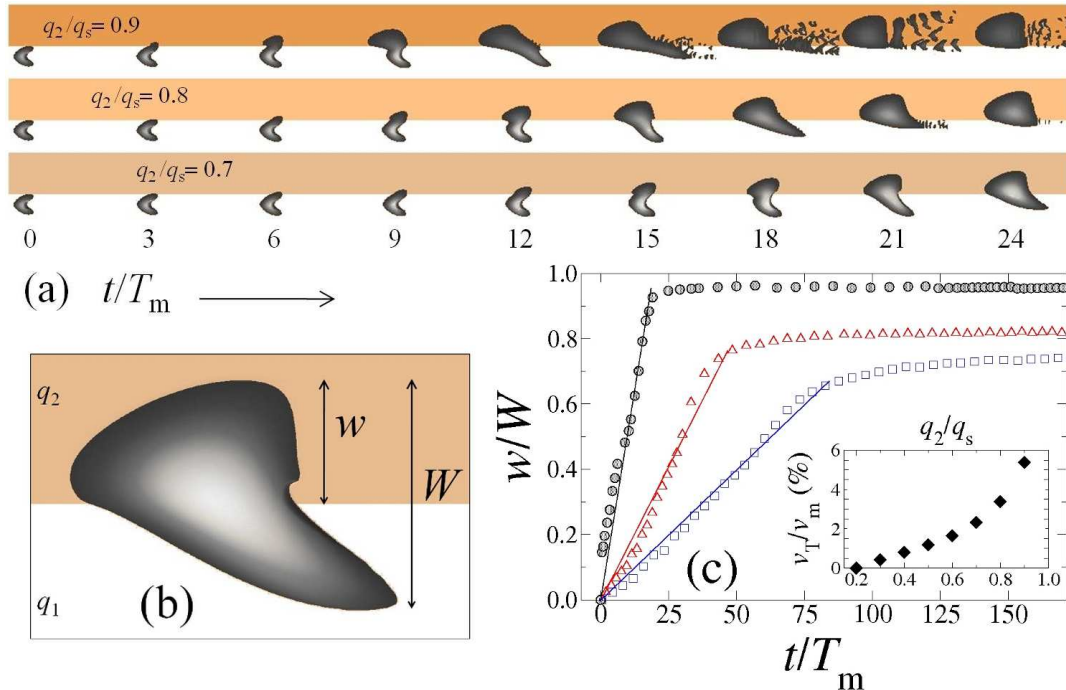


Figure 7: (a) Time evolution of a barchan of width 80 m subject to an asymmetric influx: The influx is $q_1 = 20\%$ of q_s in the white areas, in the dark areas the influx is q_2 , where $q_2/q_s = 90\%$, 80% and 70% , respectively from top to bottom. The wind blows from the left with upwind shear stress $\tau = 3.24\tau_t$. Snapshots at time interval $\Delta t = 3T_m$ where T_m is the turnover time of the barchan at $t = 0$. (b) w is the partial fraction of the barchan that is within the stream of larger influx ($q_2 = 0.7$, $t = 22T_m$), whereas W is the total width of the barchan. (c) Main plot: w/W as a function of time for $q_2/q_s = 0.4$ (squares), 0.6 (triangles) and 0.9 (circles). The straight lines are the best fits to the simulation data using a linear relation $w/W = kt/T_m$, where $k = v_T/v_m$ and v_T denotes the rate with which w/W changes with time in order to accommodate the asymmetric influx condition. The inset shows that v_T is less than 10% of v_m .

collision. Therefore, application of our results to the field should be made with care, since we did not account for the effect of dune collisions or influx asymmetry, which can influence the dune shape and will be addressed separately in later sections.

Future studies should focus on the asymmetric dune resulting from simulations using different angles between ridge orientation and wind direction, as well as different shapes of the ridge. Indeed, the results of our calculations should be valid for ridges which have a smooth cross section, where the slope of the surface does not exceed the critical angle for causing flow separation (about 20°) (Sweet and Kocurek, 1990). If the ridge's cross section has a sharp edge, then flow separation occurs and the flow is diverted parallel to the ridge along the lee side (Tsoar, 2001). In this case, sand can be transported in the direction parallel to the ridge wherever the wind speed within the separation zone exceeds the transport threshold. Moreover, the size of the zone of recirculating flow increases with the crest-to-brink distance of transverse ridges (Schatz and Herrmann, 2006), and thus the effect of secondary flow on the lateral transport of sand at the lee of the ridge should also depend on the shape of the ridge at its windward side. However, due to the assumption of our

model that net flow ceases within the separation zone, the sand deposited at the lee of a ridge with sharp edge cannot be transported at all. Thus, three-dimensional flow patterns at the lee of dunes or obstacles should be accounted for in the modeling of dune asymmetry when the topographic rise has a sharp slope (Tsoar, 2001).

5. Asymmetric sand supply

The role of asymmetric sediment supply for barchan asymmetry has remained uncertain in the few investigations undertaken (Rim, 1958; Lancaster, 1982; Bourke, 2010). It is admittedly a difficult task to conduct systematic field studies on the barchan shape as a function of the degree of spatial asymmetry in the upwind sediment budget. The sand flux onto the windward side of a barchan is largely dependent upon the spatial distribution of the upwind dunes or other sand sources, e.g. at a sand sea margin (Lancaster, 1982). Spatial inhomogeneities in the local physical properties of the interdune terrain may also play an important role for the incoming flux (Fryberger et al., 1984). Furthermore, the shape of a barchan migrating in a field is inevitably affected by wind trend variations in time (Elbelrhiti et al., 2005), as well as by the interaction

with neighbouring dunes through merging, breeding and lateral linking.

With the help of simulations, the barchan shape resulting from asymmetric upwind flux alone can be studied without regard to other physical factors. We consider a symmetric barchan initially migrating within an area where the influx q_1 is approximately a constant fraction ($\approx 20\%$) of the saturated flux (q_s) — the value of $q_1/q_s \approx 0.2$ is, in fact, within average values measured at interdune areas in typical barchan dune fields (Fryberger et al., 1984). The barchan has height $H \approx 6.0$ m and width 80 m, and has been shaped by a constant shear stress $\tau \approx 3.24\tau_t$.

At $t = 0$, the upwind influx becomes asymmetric. The influx on the side of the barchan’s left limb has a larger value, $q_2 > q_1$ (dark areas in Fig. 7a). This model for asymmetric influx constitutes a simple model for a scenario typical for real dune fields, where in some areas the presence of a dome, a sand sheet or a larger dune upwind may significantly increase the local interdune flux. Figure 7a shows different snapshots of the evolution of the barchan dune subject to the asymmetric influx. Because more sand deposits in the areas of larger influx (q_2), the dune adapts to the asymmetric influx by increasing its relative volume within the areas under influx q_2 . Different (transient) asymmetric dune shapes appear as the dune reforms its shape in order to accommodate the larger influx q_2 , as can be seen in Fig. 7a. The shorter limb is the one exposed to the larger influx value, because a large upwind flux prevents erosion at the windward foot and downwind motion of the dune. Thus, the barchan limb on the side of lower influx appears advanced in relation to its — “fat” (Long and Sharp, 1964; Parteli et al., 2007) — counterpart.

The fraction of the dune width (w/W , cf. Fig. 7b) that is within the area of larger influx (q_2) increases in time, as can be seen in Fig. 7c. In this figure, v_T denotes the rate with which w/W grows in time. Firstly, w/W increases roughly as a linear function of time which means that in this initial stage v_T is approximately constant for given values of q_1 and q_2 relative to q_s . The inset of Fig. 7c shows that v_T is indeed much smaller than the longitudinal migration velocity of the barchan (v_m) even for large q_2/q_s . Indeed, the main plot of Fig. 7c suggests that, after a sufficiently long time, w/W asymptotically approaches a maximal value (and thus $v_T \rightarrow 0$). Since the increase of w/W with time becomes extremely slow after long time, and since the dune is increasing rapidly in volume as q_2 approaches q_s , it is difficult to reliably estimate the steady-state value of w/W through numerical simulations. However, we can approximately estimate the steady-state value of w/W (which we call w_∞/W) by means of a simple calculation, as we will explain in the next paragraph.

A barchan under constant influx q_{in} is an unstable object. While the dune is gaining sand due to q_{in} , it is also losing mass through the limbs. The mass balance determines whether the dune grows or shrinks with time. As

shown previously (Durán et al., 2010), there is a critical value of q_{in} , denoted by q_c , above which the dune volume increases in time and below which the dune shrinks. This critical influx is approximately equal to 18% of the saturated flux, q_s (Durán et al., 2010). The rate dW/dt at which the cross-wind width W of the barchan changes in time approximately scales with $[q_{in} - q_c]/W$ (Durán et al., 2010). Using this relation, we can approximately estimate the growth rate of w and of $W - w$, which denote the fractions of the dune width under influx values q_2 and q_1 , respectively (cf. Fig. 7b). The growth rates dw/dt and $d(W - w)/dt$ should be proportional to $[q_2 - q_c]/w$ and $[q_1 - q_c]/(W - w)$, respectively. The steady-state value of w , i.e. w_∞ is achieved when both rates equal, which gives,

$$\frac{w_\infty}{W} = \frac{q_2 - q_c}{q_1 + q_2 - 2 \cdot q_c}, \quad (11)$$

with $q_c \approx 0.18 q_s$ as mentioned above. Figure 8 shows how w_∞/W depends on q_2/q_s for different values of q_1/q_s , with $q_1, q_2 > q_c$. For values of q_1 close to q_c , w_∞/W approaches unity as q_2 increases, which means that the dune enters almost entirely into the region of larger influx and is nearly symmetric again. This situation is indeed observed in the simulation (see e.g. Fig. 7a for $q_2/q_s = 0.9$). However, as the influx becomes very large the barchan shape gives place to a flat dome-like dune without slip-face, which may serve as source of sand for smaller dunes (Durán et al., 2010; Luna et al., 2011, 2012). We note that an increase of q_1 implies a decrease in the influx asymmetry, since q_2 is within the range $q_1 < q_2 < q_s$. Thus, as q_1 increases, the steady-state shape of the dune becomes less symmetric (though the barchan shape gives place to a dome as discussed above) and $w_\infty/W \rightarrow 0.5$. Evidently, for $q_1 = q_2$ there is no asymmetry in the influx and the dune shape is thus symmetric (w_∞ is equal to $W/2$).

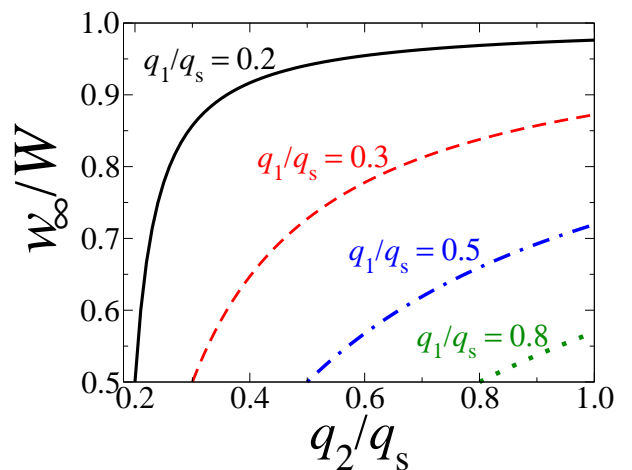


Figure 8: Steady-state value w_∞/W of the fraction w/W of the dune cross-wind width within the region of larger influx (q_2), as a function of q_2/q_s for different values of q_1/q_s .

6. Dune collisions

Dune collisions are well-known factor for the emergence of complex, asymmetric dune morphologies (Tsoar, 2001; Bourke, 2010; Ewing and Kocurek, 2010). The dynamics of collisions between two barchans have been systematically investigated in previous studies using the present model (Schwämmle and Herrmann, 2003; Durán et al., 2005, 2009). It was shown that, if the symmetry axes of both dunes are aligned, then the collision dynamics is determined by the volume ratio of the dunes, whereas the resulting morphology is symmetric (Durán et al., 2005). However, if the collision occurs with a lateral offset (cf. Fig. 9), asymmetric dune shapes can arise (Close-Arceuduc, 1969; Hersen and Douady, 2005; Durán et al., 2009).

Figure 10 shows snapshots of calculations using different values of volume ratio and lateral offset — defined as $\Delta = |Y - y|/(W/2)$, where Y (y) is the crest’s position of the large (small) dune in the direction orthogonal to the wind, and W is the width of the large dune (Fig. 9). The asymmetric dune shapes produced due to collisions are different from the ones in Section 5, since the collision not only implies an asymmetric influx but also leads to a (dynamic) modification in the shear stress field during the interaction between the dunes (Durán et al., 2005). The hybrid, asymmetric dunes depicted in Fig. 10 are transient shapes. A sufficiently long time after the collision, dunes are well separated and adapt to constant influx and wind direction again. This time-scale which the dune needs to adapt its shape after the collision is governed by the dune reconstitution time, T_m , which scales with the barchan’s cross-wind width W divided by its migration velocity v_m (Hersen et al., 2004; Durán et al., 2010). Within this time-scale, the dune migrates a downwind distance of the order of its own width W .

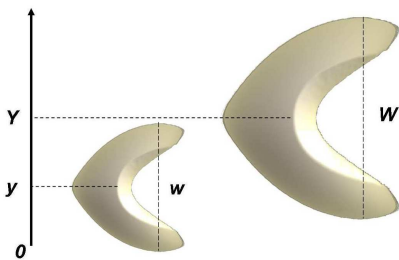


Figure 9: Binary collision between barchans of different sizes. A small barchan (width w) approaches a larger one (width W) from behind with lateral offset. The small and the large barchans are centered at y and Y , respectively.

The simulations corroborate previous observations that dune asymmetry could result from limb merging as two barchans link laterally, thereby causing downwind extension of the coalesced limbs (Bourke, 2010). Such a situation is found for sufficiently large offset ($\Delta > 0.9$), as can



Figure 10: Snapshots of simulations of binary collisions for different values of Δ and volume ratio $r \propto (w/W)^3$. Calculations with $r = 0.06$ are shown for (a) $\Delta = 0.2$, (c) $\Delta = 0.6$ and (e) $\Delta = 0.9$; calculations with $r = 0.3$ are shown for (b) $\Delta = 0.2$, (d) $\Delta = 0.6$ and (f) $\Delta = 0.9$.

be seen in Figs. 10e and 10f. It is interesting to notice that the result of the lateral coalescence is the release of a small dune from the merged limbs, whereas the colliding barchans merge then into a single asymmetric dune. The release of the small dune from the merged limbs is signature of the so-called “solitary wave-like behaviour” of sand dunes discussed in previous studies of binary collisions between barchans (Schwämmle and Herrmann, 2003; Durán et al., 2005). As the smaller, faster dune approaches the larger one from the upwind, sand from the downwind dune is trapped in the wake of its companion. Thus, the smaller dune upwind gains sand from the downwind dune thereby increasing in volume and becoming slower. Due to erosion downwind of the smaller dune’s wake region (i.e. after the “separation bubble” of the small dune), a small dune is released from the larger barchan. In effect what happens is that the colliding dunes merge to form a single (asymmetric) dune while a small barchan is ejected from the surface of the downwind dune.

Moreover, we see in Figs. 10e,f that the volume ratio of dunes colliding with large offset can yield distinct asymmetric dune shapes. If the upwind dune is small, it merges laterally to the lowest portions of the downwind barchan’s limb which is involved in the collision (cf. Fig. 10e). This limb appears then deformed (with a somewhat “sinuous” shape) and its cross-wind width also increases. However, no significant limb extension in the wind direction occurs, as we can see in the last frame of Fig. 10e. A different situation occurs if the size of the upwind dune participating at the collision is large, as in the simulation of Fig. 10f. As we can see in the last frame of this figure, the upper limb of the larger barchan left behind (i.e. the limb *opposite* to the

side where the binary collision occurred) appears *advanced* downwind. The reason for this behaviour is that the lower limb is much larger and slower than the upper one, thus appearing “retarded” in relation to its companion.

Asymmetric dune patterns very different from the ones in Fig. 10 can result from collisions between multiple dunes. Figure 11a shows one snapshot of the simulation of a barchan dune field emerging from a flat sand surface subjected to a saturated influx. The simulations of the genesis of barchan fields were discussed in detail in previous works (Durán et al., 2010; Luna et al., 2011, 2012). As shown in these works, the small transverse bedforms emerging from the instabilities which develop on the flat hill upwind give place to small barchans after reaching the bedrock — due to the cross-wind instability inherent to transverse dunes (Reffet et al., 2010; Parteli et al., 2011; Melo et al., 2012; Niiya et al., 2012). The barchan dunes, which are subjected to a strong influx, grow in size during their migration, thereby experiencing multiple collisions with their counterparts and producing complex, asymmetric dune shapes. Different patterns produced in the simulation include limb extension of the upwind barchan, as we can see in Fig. 11a. While the simulation of Fig. 11a denotes a model for an immature dune field (which is at the early stages of its development), we have also performed simulations using periodic boundary conditions in the wind direction such as to model the steady-state dynamics of a dune corridor (Durán et al., 2010). Such simulations also lead to asymmetric barchan shapes which cannot be obtained with binary collisions (cf. Fig. 11b).

The complex asymmetric shapes shown in Figs. 11a and 11b result from collisions between multiple barchans which have different sizes and offset values, and are further subjected to an asymmetric influx depending on the spatial distribution of dunes upwind. The systematic study of collisions between multiple dunes in a field is out of the scope of the present study. However, on the basis of our calculations, we can conclude that binary collisions can produce a rather limited range of asymmetric dune patterns. The only previously reported asymmetric pattern produced by a binary collision is the limb elongation due to dunes merging laterally (Fig. 10e,f). Other asymmetric patterns induced by collisions can result if the collisions involve multiple dunes during the evolution of a barchan dune field. As can be seen in Figs. 11a and 11b, collisions between dunes lead to the formation of groups of barchans, in which upwind barchans releasing sand through their extended limbs act as source of sediment to the dunes in the front, as previously noted by Tsoar (2001). Indeed, the complex patterns emerging from collisions between barchans are transient dune shapes, as shown in Fig. 10 and in previous works (Schwämmle and Herrmann, 2003; Durán et al., 2005, 2010). Further modeling work is required in order to deepen our understanding of the collision dynamics of multiple dunes and of the resulting dune patterns.

7. Discussion

The results of our simulations can help researchers in the future to discern among the most relevant factors competing for diverse types of barchan asymmetry.

For instance, our model predicts that only asymmetric bimodal wind regimes can lead to seif dune formation due to an elongating barchan limb (cf. Section 3 and the condition for seif dune elongation in Eq. (8)). Barchans subjected to an asymmetric influx, crossing a topographic rise or undergoing a collision with other dunes can experience different types of limb extension, however a seif dune cannot appear from an asymmetric barchan due to these factors alone. Furthermore, our simulations show that topographic breaks in slope and collisions can trigger extension of one or the other limb depending on the location of the dune relative to the topographic obstacle or to the surrounding dunes (cf. Figs. 6, 10 and 11). In contrast, dunes subjected to the same asymmetric bimodal wind regime should elongate the same limb, provided other asymmetry causes are not influencing the dune morphology.

Application of the results of this paper to the field should be made with care because typically asymmetric barchans result from the concurrent action of more than one asymmetry causes. In the present paper, we list three examples of barchan dunes displaying different asymmetric shapes, the origin of which could be attributed to one specific asymmetry cause, based on our simulations. These examples are discussed separately in Sections 7.1–7.3, while in Section 7.4 we discuss on how our findings could help the research of extraterrestrial dunes.

7.1. First example: barchan asymmetry induced by an asymmetric bimodal wind regime

The dune shown in Fig. 12b is in Bir Lahfan and provides an example of seif dune formation from a barchan dune due to obtuse bimodal wind regime (Tsoar, 1978, 1983, 1984, 2001). The sand rose in the inset shows two main wind directions with a divergence angle about 100° . We see that the dune displays only one limb, which aligns nearly longitudinally to the resultant transport trend. The growth and migration of the longitudinal seif dunes in Bir Lahfan was discussed in detail in previous publications (see e.g. Tsoar (1978) for a review).

The dune in Fig. 12a was obtained from a simulation using an asymmetric bimodal wind regime with $r = 50\%$. It is the third dune from left to right in Fig. 4a bottom ($q_{in} = 20\%$ of the saturated flux). This dune indeed displays some characteristics that are found in the real Bir Lahfan dune, namely it has only one limb, which is elongating into a seif dune.

The wind regime that generated the dune of Fig. 12a differs from the one in the sand rose of Fig. 12b as in this sand rose both main wind directions have nearly equal transport rates. Indeed, it was shown in experiments (Reffet et al., 2010) and numerical simulations (Parteli et al., 2009), that symmetric bimodal flow regimes (with $r = 100\%$) lead

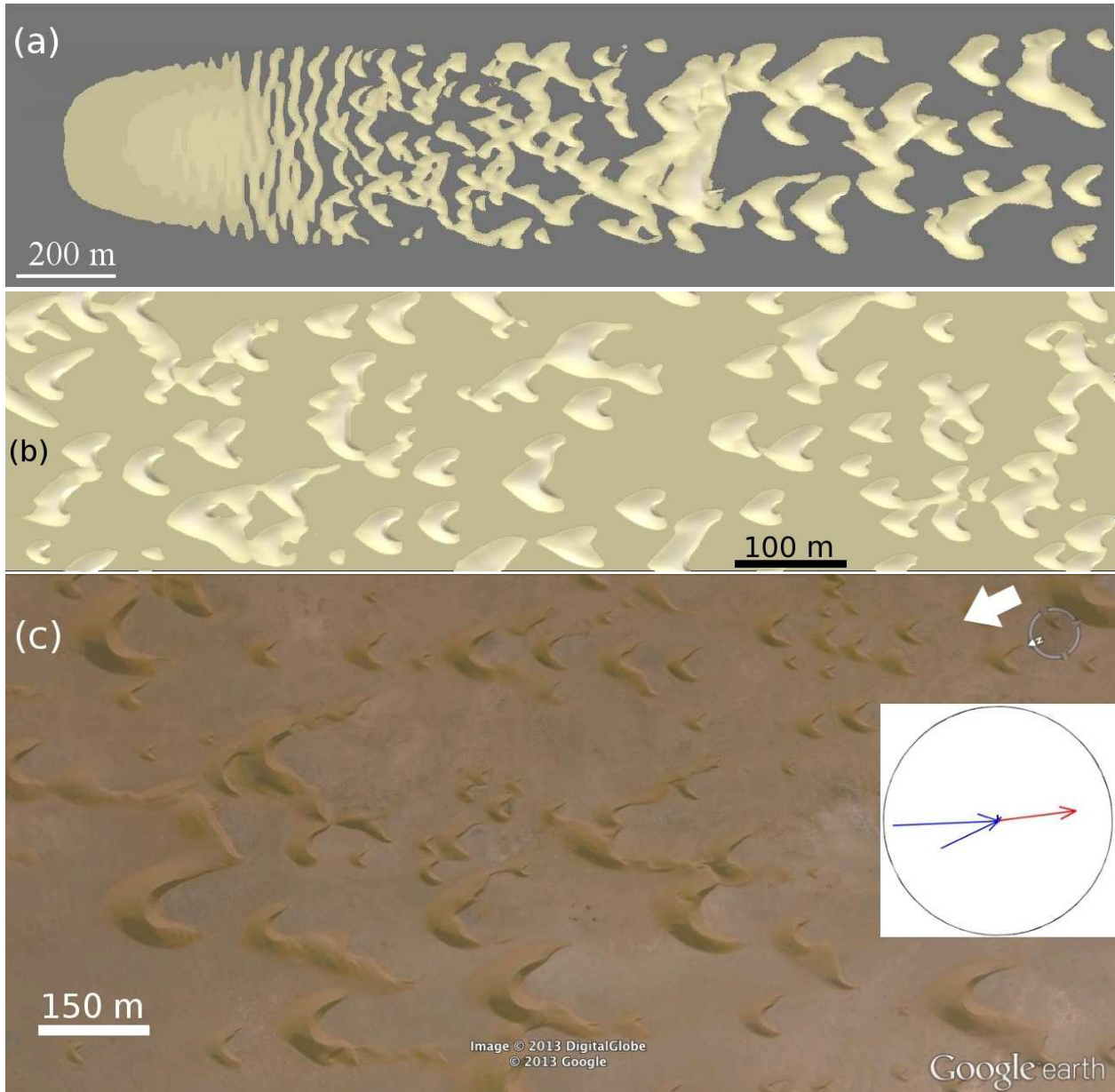


Figure 11: Asymmetric barchans emerge during the evolution of a barchan dune field. (a) Simulation of the genesis of a dune field. A small, flat sand hill subjected to saturated flux becomes a source of sand for a barchan dune field (Durán et al., 2010; Luna et al., 2012). Collision between multiple dunes lead to complex asymmetric dune morphologies which are not obtained in binary collisions (cf. Fig. 10). (b) Complex asymmetric barchan shapes also occur in the simulation of a barchan corridor using periodic boundary conditions both in the direction perpendicular and parallel to the wind. Wind blows from left to right in both (a) and (b). Simulations were performed with $\tau/\tau_t \approx 3.9$. (c) Barchan dunes in Morocco, located at $26^\circ 47' 02.81''\text{N}$, $13^\circ 22' 42.16''\text{W}$ (image credit: Google Earth). The north direction is indicated by the arrow at the top-right corner. The sand rose in the inset at right is for El Aaiun, which is located near $27^\circ 09'\text{N}$, $13^\circ 12'\text{W}$, about 42 km from the dunes in the image.

to *symmetric* longitudinal dunes rather than asymmetric barchans. However, we note that the sand rose in Fig. 12b also displays secondary transport directions, which are not taken into account in the simulations. The role of these smaller transport directions for the dune shape is still uncertain. Simulations using multidirectional wind regimes,

which are out of the scope of the present work, should be performed in the future in order to clarify the relevance of secondary transport directions for the shape and elongation of asymmetric barchans.

Possibly, the presence of more than two wind directions as well as influx asymmetry due to the presence of other

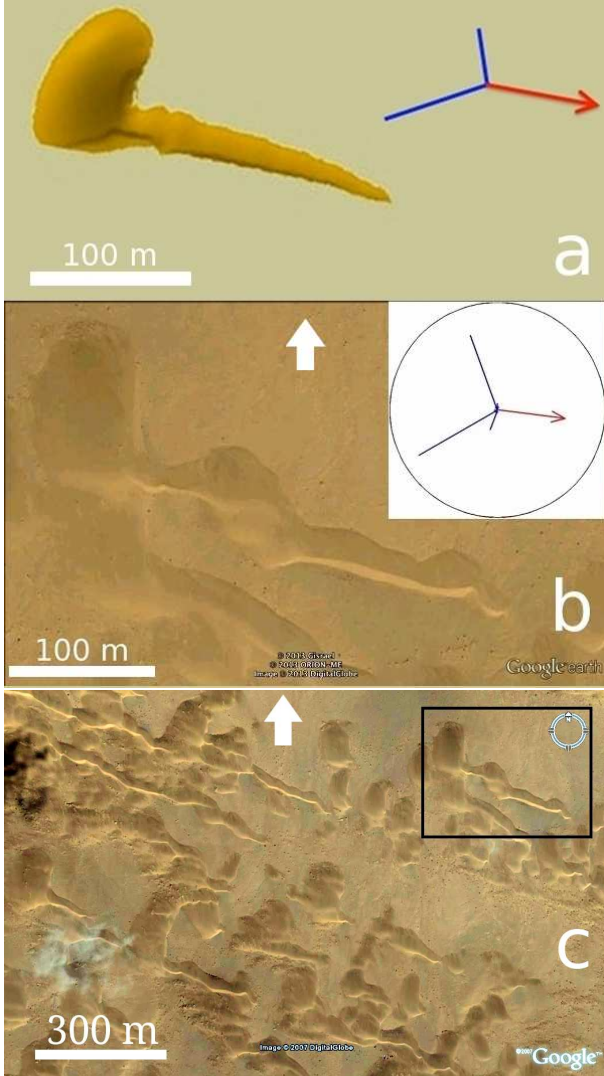


Figure 12: Barchan asymmetry due to an asymmetric wind regime. In (a) we see a dune obtained in simulation using a bimodal wind regime with $r = 50\%$ and $t_1 = 0.1$ (see Fig. 4a). The influx is $q_{in} = 20\%$ of the saturated flux. We compare this dune with the asymmetric barchan in (b), which is at Bir Lahfan in Sinai, near $30^{\circ}51'04.03''N$, $33^{\circ}52'24.19''E$. The sand rose shown in the inset is for an area between Bir Lahfan and Jabel Libni, Sinai. (c) Image of the dune field at Bir Lahfan showing that the dune in (b), enclosed by the box, is surrounded by other asymmetric barchans which are also giving rise to seif dunes. Both in (b) and (c), north is at top as indicated by the arrows (images credit: Google Earth).

dunes in the field (see Fig. 12c) could explain the meandering of the barchan limb visible in Fig. 12b. This meandering is namely absent from the asymmetric barchan of Fig. 12a and also from symmetric longitudinal dunes on top of bedrock generated in experiments (Reffet et al., 2010) and numerical simulations (Parteli et al., 2009).

7.2. Second example: barchan asymmetry induced by topography

The second example is provided in Fig. 6a, which shows asymmetric barchans in Peru, while the sand rose of the dune field is shown in the inset. The barchans are crossing topographic rises, which suggests topography as cause for their asymmetric shape (Bourke, 2010). Indeed, as discussed in Section 4, we found that when the barchans are *upwind* of the ridge's crest, the limb closest to the ridge appears extended, while the other limb elongates once the dune has crossed the ridge, i.e. when the dune is *downwind* of the ridge's crest (see Fig. 6c). Although this behavior could explain the asymmetric shape of some of the dunes in Fig. 6a (in particular see the simulation of Fig. 6b and the more detailed discussion in Section 4), for many of the dunes in Peru other asymmetry causes cannot be excluded, in particular collisions (Bourke, 2010).

7.3. Third example: barchan asymmetry induced by collisions

We see in Fig. 11c the third example of barchan asymmetry, which is caused by collisions. Many of the dunes in Fig. 11c that are well separated from other dunes, and are thus not participating of a collision, have approximately the same shape, which is nearly symmetric and consistent with the wind regime indicated by the sand rose in the inset. Other dunes in the barchan corridor, especially those migrating close to other dunes, display different types of asymmetry. We see that several barchans have the upper limb extended, while others have the lower limb extended. Moreover, in some cases either limb is giving rise to a small barchan, thus indicating that dune *calving* (Durán et al., 2005; Génois et al., 2013; Worman et al., 2013) is a relevant mechanism for the generation of small dunes in the field. The simulations of Figs. 11a and 11b, performed with strictly unidirectional wind regimes (wind blows from left to right), produce barchan asymmetry behavior with the characteristics found in the examples of Fig. 11c, thus indicating that complex (asymmetric) wind regimes are not a pre-requisite for the asymmetric dune shapes in the referred field.

7.4. Application of the model to the research of extraterrestrial dunes — a discussion

Asymmetric barchan dunes occur in many dune fields on Mars (Bourke et al., 2004; Bourke and Goudie, 2009; Bourke, 2010). It was shown by Bourke (2010) that the origin of a variety of Martian asymmetric barchans could be understood on the basis of the four main asymmetry causes tested in the present paper. Indeed, the insights of our simulations should be applicable for understanding the formation of seif dunes on Mars and also the influence of topography and collisions on complex dune patterns occurring within Martian barchan corridors.

In Martian dune fields hosting asymmetric barchans with one limb elongating into a seif dune, Figs. 3 and 4

could be used for estimating the divergence angle θ_w and the ratio r between the transport rates associated with the dominant sand-moving wind directions. We note that a diversity of exotic Martian dune shapes occurring on top of bedrock could be indeed simulated with the present model using obtuse bimodal wind regimes with $r = 1.0$ (Parteli and Herrmann, 2007; Parteli et al., 2009). On the other hand, due to the lower gravity of Mars the influence of topography on the shape of barchan dunes on the red planet should be correspondingly smaller than on Earth. For instance, we expect dunes crossing a sloping terrain on Mars to migrate laterally as they do on Earth, however the value of k_q (cf. Eq. (9)), which gives the ratio of transverse to longitudinal migration rates, should be smaller on Mars for a given terrain's slope. Furthermore, simulations of dune collisions such as the ones in Figs. 10 and 11 but using attributes of sediment and fluid valid for Martian sand systems could shed light on the origin of complex asymmetric patterns occurring on different locations (and thus environmental conditions) on Mars. However, in order to perform quantitative simulations, the model should be further improved by accounting for recently noted differences between saltation on Mars and Earth as well as for the recently gained insights into the physics of the threshold wind velocity required to sustain sediment transport on Mars (Almeida et al., 2008; Kok, 2010). Moreover, future simulations should incorporate a model for the saturation length ℓ_s (cf. Eq. (5)) that encodes the relevant mechanisms of flux saturation of sediment transport in extraterrestrial environments (Pächt et al., 2013).

Finally, asymmetric barchans leading to seif dunes due to limb extension could be identified in Cassini images of the surface of Titan (Radebaugh et al., 2010), thus indicating asymmetric bimodal wind regimes on this Saturn's moon. The formation of the equatorial linear dune fields of Titan has been indeed attributed to seasonally varying winds (Lorenz et al., 2006; Tokano, 2010). Thus, the modeling presented here could be used to investigate the ratios of transport rates and divergence angles of Titan's bimodal wind regimes at those locations hosting asymmetric barchans.

8. Conclusions

In conclusion, we have investigated, by means of morphodynamic modeling of aeolian dunes, the respective roles of bimodal wind regimes, topography, influx asymmetry and dune collisions on the formation and evolution of asymmetric barchan dune shapes. The conclusions of our numerical simulations can be summarized as follows:

- *Bimodal wind regimes* — the limb opposite to the secondary wind elongates into the resultant transport direction if the divergence angle of the bimodal wind is obtuse and the ratio $[Q_2 T_{w2}]/[Q_1 T_{w1}]$ — where Q_1 (Q_2) and T_{w1} (T_{w2}) stand for the bulk sand flux and

the duration of the primary (secondary) wind, respectively — exceeds 25%. These conditions are the same as the ones for oblique alignment of bedforms in dense sand beds (Rubin and Hunter, 1987), the asymmetric barchan being the corresponding morphology under low amount of available sand.

- *Topography* — a barchan crossing a topographic rise can become asymmetric; the limb closest to the topographic rise elongates downwind. The migration velocity of a barchan that is on a tilted surface has a downhill component proportional to the tilting slope; the preferential limb extension is downhill rather than downwind.
- *Influx asymmetry* — the side of the barchan subjected to the larger influx increases in volume, whereas the opposite limb elongates downwind. The typical asymmetric morphology is a barchan with an elongated arm (the one subjected to lower influx). The asymmetry is of transient nature, since the dune migrates laterally towards the region of higher influx.
- *Dune collisions* — asymmetry can be triggered due to barchan collisions with lateral offset. Binary collisions with large offset can lead to extension of the limb resulting from the merging of the two limbs participating at the collision. Collisions between multiple barchans in a field can trigger more complex asymmetric patterns. Some patterns produced in these simulations involve the elongation of one limb of the upwind dune, as reported from previous observations (Bourke, 2010).

In order to improve the quantitative assessment of asymmetric barchans, the model should be extended in order to account for secondary flow effects at the dune lee (Tsoar, 2001), which may be relevant for the dynamics of limb elongation due to bimodal wind regimes or due to topographic ridges with sharp slopes (Bourke, 2010). Indeed, the separation bubble model of Section 2.1 does not account for the occurrence of three-dimensional flow structures within the zone of recirculating flow, which affect the dune shape at the lee and can contribute to the elongation of the limb. Realistic simulations of bimodal wind regimes should further account for multiple secondary wind trends in consistence with the complex sand roses of real dune fields (Fryberger and Dean, 1979). Moreover, real winds can be very gusty, with changes in direction of 45 degrees or more taking place in most cases in less than 15 minutes, while in some instances the changes may be gradual or abrupt (Elbelrhiti et al., 2005; Durán et al., 2011). This effect of changes in wind directions should be considered in the future. Finally, we also note that there are examples of seif dunes formation from vegetated linear dunes that lost their vegetation due to human impact (Tsoar, 2001). The formation of seif dunes in the presence of a dynamic vegetation cover remains to be investigated in the future.

The results of our calculations are potentially useful for inferring local wind regimes or spatial variations either in topography or in availability of mobile sediments in planetary dune fields where asymmetric barchans occur.

Acknowledgments

This work was supported in part by NASA MDAP Grant NNX10AQ35G, by FUNCAP, CAPES and CNPq (Brazilian agencies), by FUNCAP Grant 0011-00204.01.00/09, by Swiss National Foundation Grant NF 20021-116050/1 and ETH Grant ETH-10 09-2. We also thank the German Research Foundation (DFG) for funding through the Collaborative Research Initiative “Additive Manufacturing” (SFB814) and the Cluster of Excellence “Engineering of Advanced Materials”.

References

Allen, J.R.L., 1974. Reaction, relaxation and lag in natural sedimentary systems: General principles, examples and lessons. *Earth Sci. Rev.* 10, 263-342.

Almeida, M.P., Parteli, E.J.R., Andrade Jr., J.S., Herrmann, H.J., 2008. Giant saltation on Mars. *Proc. Natl. Acad. Sci.* 105, 6222-6226.

Andreotti, B., 2004. A two-species model of aeolian sand transport. *Journal of Fluid Mechanics* 510, 47-70.

Araújo, A.D., Parteli, E.J.R., Pöschel, T., Andrade Jr., J.S., Herrmann, H.J., 2013. Numerical modeling of the wind flow over a transverse dune. *Scientific Reports* 3, 2858. doi:10.1038/srep02858.

Bagnold, R.A., 1941. *Physics of blown sand and desert dunes*. Methuen, London, 289 pp.

Bourke, M.C., Balme, M., Zimbelman, J.R., 2004. A comparative analysis of barchan dunes in the intra-crater dune fields and the North Polar Sand Sea, LPSC XXXV abstr. #1453.

Bourke, M.C., 2010. Barchan dune asymmetry: Observations from Mars and Earth. *Icarus* 205, 183-197.

Bourke, M.C., Goudie, A.S., 2009. Varieties of barchan dunes in the Namib Desert and on Mars. *Aeolian Research* 1, 45-54.

Bourke, M.C., Lancaster, N., Fenton, L.K., Parteli, E.J.R., Zimbelman, J.R., Radebaugh, J., 2010. Extraterrestrial dunes: An introduction to the special issue on planetary dune systems. *Geomorphology* 121, 1-14.

Bristow, C.S., Bailey, S.D., Lancaster, N., 2000. The sedimentary structure of linear sand dunes. *Nature* 406, 56-59.

Close-Arceuduc, A. *Essai d'explication des formes dunaires sahariennes*. Etudes de Photo-Interpretation. Institut Geographique National, 1969.

De Hon RA, 2006. Transitional Dune Forms on Mars. *Proc. Lunar Planet. Sci. Conf.* 37, #1361.

Dong, Z., Wei, Z., Qian, G., Zhang, Z., Luo, W., Hu, G., 2010. “Raked” linear dunes in the Kumtagh Desert, China. *Geomorphology* 123, 122-128.

Durán, O., Schwämmle, V. and Herrmann, H.J., 2005. Breeding and solitary wave behavior of dunes. *Physical Review E* 72, 021308.

Durán, O., Herrmann, H.J., 2006a. Modelling of saturated sand flux. *Journal of Statistical Mechanics: Theory and Experiment*, P07011.

Durán, O., Herrmann, H.J., 2006b. Vegetation against dune mobility. *Physical Review Letters* 97, 188001.

Durán, O., Schwämmle, V., Lind, P.G., Herrmann, H.J., 2009. The dune size distribution and scaling relations of barchan dune fields. *Granular Matter* 11, 7-11.

Durán, O., Parteli, E.J.R., Herrmann, H.J., 2010. A continuous model for sand dunes: Review, new developments and application

to barchan dunes and barchan dune fields. *Earth Surface Process and Landforms* 35, 1591-1600 (2010). doi:10.1002/esp.2070.

Durán, O., Claudin, P., Andreotti, B., 2011. On aeolian transport: Grain-scale interactions, dynamical mechanisms and scaling laws. *Aeolian Research* 3, 243-270.

Elbelrhiti, H., Claudin, P., Andreotti, B., 2005. Field evidence for surface-wave-induced instability of sand dunes. *Nature*, 437, 720-723.

Ewing, R.C., Kocurek, G.A., 2010. Aeolian dune interactions and dune-field pattern formation: White Sands Dune Field, New Mexico. *Sedimentology* 57, 1199-1219. doi:10.1111/j.1365-3091.2009.01143.x.

Finkel, H.J., 1959. The barchans of southern Peru. *J. Geol.* 67, 614-647.

Fryberger, S.G., Dean, G., 1979. A Study of Global Sand Seas. In: McKee, E.D. (Ed.), *U.S. Geol. Surv. Prof. Pap.*, 1052. U.S. Geological Survey, Reston, VA, pp. 137-169.

Fryberger, S.G., Al-Sari, A.M., Clisham, T.J., Rizvi, S.A.R., Al-Hinai, K.G., 1984. Wind sedimentation in the Jafurah sand sea, Saudi Arabia. *Sedimentology* 31, 413-431.

Gay, S.P., 1999. Observations regarding the movement of barchan sand dunes in the Nazca to Tanaca area of southern Peru. *Geomorphology* 27, 279-293.

Génois, M., Du Pont, S.C., Hersen, P., Grégoire, G., 2013. An agent-based model of dune interactions produces the emergence of patterns in deserts. *Geophysical Research Letters* 40, 3909-3914.

Goudie, A., Wilkinson, J., 1977. *The warm desert environment*. Cambridge Univ. Press, Cambridge, 88 pp.

Herrmann, H.J., Andrade Jr., J.S., Schatz, V., Sauermann, G., Parteli, E.J.R., 2005. Calculation of the separation streamlines of barchans and transverse dunes. *Physica A* 357, 44-49.

Hersen, P., Andersen, K.H., Elbelrhiti, H., Andreotti, B., Claudin, P., Douady, S., 2004. Corridors of barchan dunes: Stability and size selection. *Physical Review E* 69, 011304.

Hersen, P., Douady, S., 2005. Collision of barchan dunes as a mechanism of size regulation. *Geophys. Res. Lett.* 32, 1-5.

Iversen, J.D., White, B.R., 1982. Saltation threshold on Earth, Mars and Venus. *Sedimentology* 29, 111-119.

Kok, J.F., 2010. Difference in wind speeds required for initiation versus continuation of sand transport on Mars: Implications for dunes and dust storms. *Physical Review Letters* 104, 074502.

Kok, J.F., Parteli, E.J.R., Michaels, T.I., Bou Karam, D., 2012. The physics of wind-blown sand and dust. *Reports on Progress in Physics* 75, 106901.

Kroy, K., Sauermann, G., Herrmann, H.J., 2002. Minimal model for aeolian sand dunes. *Physical Review E* 66, 031302.

Lancaster, N., 1980. The formation of seif dunes from barchans — supporting evidence for Bagnold’s model from the Namib Desert. *Zeitschrift für Geomorphologie N.F.* 24, 160-167.

Lancaster, N., 1982. Dunes on the Skeleton Coast, Namibia (south west Africa): Geomorphology and grain size relationships. *Earth Surf. Proc. Land.* 7, 575-587.

Lancaster, N., 1988. The development of large aeolian bedforms. *Sediment Geology* 55, 69-89.

Long, J.T., Sharp, R.P., 1964. Barchan-dune movement in Imperial Valley, California. *Geol. Soc. Am. Bull.* 75, 149-156.

Lorenz, R.D., *et al.*, 2006. The sand seas of Titan: Cassini RADAR observations of longitudinal dunes. *Science* 312, 724-727.

Luna, M.C.M.M., Parteli, E.J.R., Durán, O., Herrmann, H.J., 2011. Model for the genesis of coastal dune fields with vegetation. *Geomorphology* 129, 215-224.

Luna, M.C.M.M., Parteli, E.J.R., Herrmann, H.J., 2012. Model for a dune field with an exposed water table. *Geomorphology* 159-160, 169-177.

Mabbutt, J.A., 1977. *Desert Landforms* (MIT Press, Cambridge), 340 pp.

McKee, E., Tibbitts, G.C., Jr., 1964. Primary structures of a seif dune and associated deposits in Libya. *Journal of Sedimentary Petrology* 34, 5-17.

Melo, H.P.M., Parteli, E.J.R., Andrade Jr., J.S., Herrmann H.J., 2012. Linear stability analysis of transverse dunes. *Physica A* 391,

- 4606-4614.
- Niyya, H., Awazu, A., Nishimori, H., 2012. Bifurcation analysis of the transition of dune shapes under a unidirectional wind. *Physical Review Letters* 108, 158001.
- Owen, P.R., 1964. Saltation of uniform grains in air. *Journal of Fluid Mechanics* 20, 225-242.
- Parteli, E.J.R., Schwämmle, V., Herrmann, H.J., Monteiro, L.H.U., Maia, L.P., 2006. Profile measurement and simulation of a transverse dune field in the Lencois Maranhenses. *Geomorphology* 81, 29-42.
- Parteli, E.J.R., Durán, O., Herrmann, H.J., 2007. Minimal size of a barchan dune. *Physical Review E* 75, 011301.
- Parteli, E.J.R., Herrmann, H.J., 2007. Saltation transport on Mars. *Physical Review Letters* 98, 198001.
- Parteli, E.J.R., Durán, P., Tsoar, H., Schwämmle, V., Herrmann, H.J., 2009. Dune formation under bimodal winds. *Proc. Nat. Acad. Sci.* 106, 22085-22089.
- Parteli, E.J.R., Andrade Jr., J. S., Herrmann, H.J., 2011. Transverse instability of dunes. *Physical Review Letters* 107, 188001.
- Pähtz, T., Kok, J.F., Herrmann, H.J., 2012. The apparent roughness of a sand surface blown by wind from an analytical model of saltation. *New Journal of Physics* 14, A262.
- Pähtz, T., Kok, J.F., Parteli, E.J.R., Herrmann, H.J., 2013. Flux saturation length of sediment transport. *Physical Review Letters* 111, 218002.
- Pye, K., Tsoar, H., 1990. *Aeolian Sand and Sand Dunes*. Unwin Hyman, London.
- Radebaugh, J., Lorenz, R., Farr, T., Paillou, P., Savage, C., Spencer, C., 2010. Linear dunes on Titan and Earth: Initial remote sensing comparisons. *Geomorphology* 121, 122-132.
- Reffet, E., Courrech du Pont, S., Hersen, P., Douady, S., 2010. Formation and stability of transverse and longitudinal sand dunes. *Geology* 38, 491-494.
- Rim, S.C.R., 1958. Simulations by dynamical model, of sand tract morphology occurring in Israel. *Bull. Res. Council. Israel* 7-G, 123-137.
- Rubin D.M., Hunter R.E., 1987. Bedform alignment in directionally varying flows. *Science* 237, 276-278.
- Rubin D.M., Ikeda, H., 1990. Flume experiments on the alignment of transverse, oblique, and longitudinal dunes in directionally varying flows. *Sedimentology* 37, 673-684.
- Rubin, D.M., Tsoar, H., Blumberg, D.G., 2008. A second look at western Sinai seif dunes and their lateral migration. *Geomorphology* 93, 335-342.
- Ruhe, R.V., 1975. *Geomorphology*. Houghton Mifflin, Boston, 246 pp.
- Sauermann, G., Kroy, K., Herrmann, H.J., 2001. A continuum saltation model for sand dunes. *Physical Review E* 64, 31305.
- Sauermann, G., Andrade Jr., J.S., Maia, L.P., Costa, U.M.S., Araújo, A.D., Herrmann, H.J., 2003. Wind velocity and sand transport on a barchan dune. *Geomorphology* 54, 245-255.
- Schatz, V., Herrmann, H.J., 2006. Flow separation in the lee side of transverse dunes: a numerical investigation. *Geomorphology* 81, 207-216.
- Schwämmle, V., Herrmann, H.J., 2003. *Nature* 426, 619-620 (2003).
- Sullivan, R., Greeley, R., Kraft, M., Wilson, G., Golombek, M., Herkenhoff, K., Murphy, J., Smith, P., 2000. Results of the imager for Mars Pathfinder windsock experiment. *Journal of Geophysical Research* 105, 24547-24562.
- Sweet, M.L., Kocurek, G., 1990. An empirical model of aeolian dune lee-face airflow. *Sedimentology* 37, 1023-1038.
- Tokano, T., 2010. Relevance of fast westerlies at equinox for the eastward elongation of Titan's dunes. *Aeolian Research* 2, 113-127.
- Tsoar, H., 1978. The Dynamics of longitudinal dunes. Final technical report, European Res. Off. U.S. Army, London, England. 171 pp.
- Tsoar, H., 1982. Internal structure and surface geometry of longitudinal (seif) dunes. *J. Sediment. Petrol.* 52, 823-831.
- Tsoar, H., 1983. Dynamic processes acting on a longitudinal (seif) sand dune. *Sedimentology* 30, 567-578.
- Tsoar, H., 1984. The formation of seif dunes from barchans — a discussion. *Zeitschrift für Geomorphologie* 28, 99-103.
- Tsoar, H., 2001. Types of Aeolian Sand Dunes and Their Formation. *Geomorphological Fluid Mechanics* 582, 403-429.
- Verstappen, H.Th., 1968. On the origin of longitudinal (seif) dunes. *Zeitschrift für Geomorphologie N.F.* 12, 200-220.
- Walker, I.J., Nickling, W.G., 2002. Dynamics of secondary airflow and sediment transport over and in the lee of transverse dunes. *Progress in Physical Geography* 26, 47-75.
- Weng, W.S., Hunt, J.C.R., Carruthers, D.J., Warren, A., Wiggs, G.F.S., Livingstone, I., Castro, I., 1991. Air flow and sand transport over sanddunes. *Acta Mechanica, Suppl.* 2, 1-22.
- Worman, S.L., Murray, A.B., Littlewood, R., Andreotti, B., Claudin, P., 2013. Modeling emergent large-scale structures of barchan dune fields. *Geology* 41, 1059-1062.